PAPER • OPEN ACCESS

Surface states characterization in the strongly interacting graphene/Ni(111) system

New Journal of Physics
The open access journal at the forefront of physics

Deutsche Physikalische Gesellschaft DPG
IOP Institute of Physics

Published in partnership with: Deutsche Physikalische Gesellschaft and the Institute of Physics

OPEN ACCESS

RECEIVED
7 August 2018

REVISED
21 September 2018

ACCEPTED FOR PUBLICATION
11 October 2018

PUBLISHED
29 October 2018

PAPER

Surface states characterization in the strongly interacting graphene/Ni(111) system

S Achilli[1], S Tognolini[2], E Fava[2], S Ponzoni[2], G Drera[2], C Cepek[3], L L Patera[3,4,6], C Africh[3], E del Castillo[5], M I Trioni[5] and S Pagliara[2]

[1] Dipartimento di Fisica, Università degli Studi di Milano, via Celoria 6, I-20133 Milano, Italy
[2] I-LAMP and Dipartimento di Matematica e Fisica, Università Cattolica, via dei Musei 41, I-25121 Brescia, Italy
[3] CNR-IOM, Laboratorio TASC, Strada Statale 14, Km 163.5, I-34149 Trieste, Italy
[4] Dipartimento di Fisica, Università di Trieste, Via A. Valerio 2, I-34127 Trieste, Italy
[5] CNR-ISTM and Dipartimento di Chimica, Università degli Studi di Milano, Via Golgi 19, I-20133 Milano, Italy
[6] Present address: Institute of Experimental and Applied Physics, University of Regensburg, D-93053 Regensburg, Germany.

E-mail: simona.achilli@unimi.it

Keywords: image potential states, graphene, Ni(111), surface states

Supplementary material for this article is available online

Abstract

By combining nonlinear photoemission experiments and density functional theory calculations, we study the modification of Ni(111) surface states induced by the presence of graphene. The main result is that graphene is able to displace the Ni(111) surface states from the valence band close to the Fermi level uncovering the *d*-band of Ni. The shift of the surface states away from the Fermi level modifies their *k*-dispersion and the effective mass. The unoccupied image state of graphene/Ni(111) has been also characterized. The *ab initio* calculations give a theoretical insight into the electronic properties of graphene/Ni(111) in the two stable top-fcc and top-bridge phases showing that the interface properties are poorly dependent on the stacking. The screening properties to an externally applied electric field are also discussed.

1. Introduction

Growing graphene on metal surfaces gives rise to a change in the electronic structure of the substrate and the overlayer whose entity defines their mutual interaction as 'weak' or 'strong', while the interaction energy is usually small [1–12].

It is known that in weakly interacting graphene/metal systems, where the graphene/metal distance is comparable with that of the graphene layers in graphite, the Dirac cone and metallic surface states appear essentially unchanged [13, 14].

In the strongly interacting systems, in which the carbon/metal separation is small, the situation is more complicated. For example, in graphene/Ru an additional image state appears, which is the most strongly bound and is characterized by a shorter lifetime and a higher effective mass. The origin of such state was explained accounting for the corrugation of the graphene layer [14].

In this light, graphene on Ni(111), growing as a flat layer with a small graphene/Ni separation (about $d = 2.1$ Å), represents a model system among the strongly interacting graphene/metal interfaces [15]. Moreover, the magnetic properties of Ni are expected to induce a magnetic character in the electronic states at this interface making graphene/Ni(111) a suitable system for application in spintronic. Considering the electronic band structure of graphene/Ni(111), the region around the $\overline{\mathrm{K}}$ point delivers the most interesting and important information with respect to the possible spin-filtering effects. Nevertheless, also the electronic structure at the $\overline{\Gamma}$ point on clean Ni(111), being dominated by spin polarized surface states, is relevant. A recent study [16] has definitively clarified the electronic structure at the $\overline{\Gamma}$ point of Ni(111). A Shockley surface state, derived from the *sp* band, with a majority spin component presides over the electronic structure at the Fermi

level, while its minority component is unoccupied. A second surface state with minority spin character, deriving from the *d*-bands also exists with its counterparts [17–19].

Moreover, an unoccupied image potential state (IPS) is present at 0.8 eV below the vacuum level, with an exchange splitting of about 14 meV, in agreement with the theoretical estimation based on the bulk penetration of the IPS wave function. While a complete and detailed study of the surface states on clean Ni(111) has been addressed [16, 17] an equivalent investigation on graphene/Ni(111) is lacking.

In this work, on the basis of linear and two-photon photoemission (2-PPE) measurements performed for both graphene-covered and clean Ni(111) surface, we are able to supply a complete characterization of electronic states close to the Fermi level of the strongly interacting model system graphene/Ni(111). In particular, 2-PPE spectroscopy, with respect to the photoemission measurements where a He lamp is employed, using a photon energy lower than the sample work function, allows to investigate both occupied and unoccupied states close to the Fermi level. The experimental results are supported by state of the art density functional theory calculations.

Being the in-plane lattice constant of the two systems very close, the unit cell of graphene matches that of Ni and the graphene/Ni(111) system can display stable domains in which the overlayer grows with perfect order at the interface. Indeed, although the formation of rotated domains is also possible, epitaxial layers aligned to the surface lattice are easily formed, with different possible stacking configurations of carbon atoms with respect to the underlying substrate. Among them the top-fcc, top-hcp, and fcc-hcp were initially proposed as the most stable ones [10], although with some controversy. Theoretical calculations, performed with different exchange and correlation functionals, identified different energetically favorable stackings [20–22]. *Ab initio* calculations including dispersion forces finally established that the top-fcc and the top-bridge are equally probable, being characterized by very similar chemisorption minima [23–25].

This was confirmed also by a series of experimental studies that demonstrated the coexistence of these phases [4, 23, 25, 26].

In the following, the characterization of the graphene/Ni(111) surface states has been carried out comparing the 2-PPE measurements with the theoretical analysis of the electronic properties for both the top-bridge and top-fcc stacking. We will show that the properties of the surface states are in general poorly dependent on the stacking configuration. Concerning the measured IPSs, the drawback of density functional theory in describing the asymptotic decay of the potential in vacuum does not allow a direct comparison with the experiments. We calculate *ab initio* the screening properties of graphene/Ni(111) that are directly related to the formation of the image potential tail. We show that the two stackings display some differences in the spin dependent polarization charge and density of states (DOS) at the Fermi level. Nevertheless the response to an external electric field is quite similar in the two configurations suggesting that also the IPSs are not affected by the local arrangement of the surface.

2. Experimental details

The epitaxial graphene was obtained using a Ni(111) crystal presenting carbon-contaminated subsurface, as defined in [27]. We recall that in this case, after the usual cleaning procedure in UHV (sputtering and annealing), as soon as the temperature is increased to 400 °C–600 °C, the formation of graphene seeds at the Ni surface is observed. Under these conditions, the graphene islands expand, fed by the C atoms from the subsurface reservoir, leading to a complete, mainly epitaxial, graphene overlayer [27]. Dosing C_2H_4 (10^{-7}–10^{-6} mbar) after the graphene nucleation increases the growth rate, without affecting the final graphene morphology. In this work, a carbon-contaminated subsurface Ni(111) substrate has been prepared upon extensive C_2H_4 dosing ($p = 10^{-7}$–10^{-6} mbar), followed by several cycles of Ar^+ sputtering at 2 KeV and flash annealing at 600 °C. This procedure was necessary to remove the surface contaminants and oxidation due to air exposure, but it was not strong enough to remove also the carbon reservoir. Then it was annealed at 550 °C for 60 minutes, back-filling the chamber with C_2H_4 (2×10^{-6} mbar), obtaining a complete epitaxial graphene monolayer, as confirmed by XPS, LEED, and UPS.

For nonlinear angle-resolved photoemission measurements, a Ti:Sapphire laser system delivering 0.6 mJ, 150 fs pulses at a wavelength of 790 nm and 1 kHz repetition rate was employed. The laser pulses were also used to pump a traveling wave optical parametric amplifier covering a wavelength corresponding to an energy range from 0.80 to 1.07 eV. By quadrupling the output of the parametric amplifier, the photon energy could be tuned continuously from 3.20 to 4.28 eV. The near-UV pulses were focused on the sample, kept in an UHV chamber at a residual pressure $< 2 \times 10^{-10}$ mbar and annealed before the photoemission experiments to 650 K to remove any physisorbed species and water resulting from transport through air. Photoelectrons were detected by means of a custom-made time of flight electron spectrometer with an angular acceptance of $\pm 0.85°$ and an overall energy resolution of ~35 meV at an electron kinetic energy of 2.0 eV. The experimental geometry and the

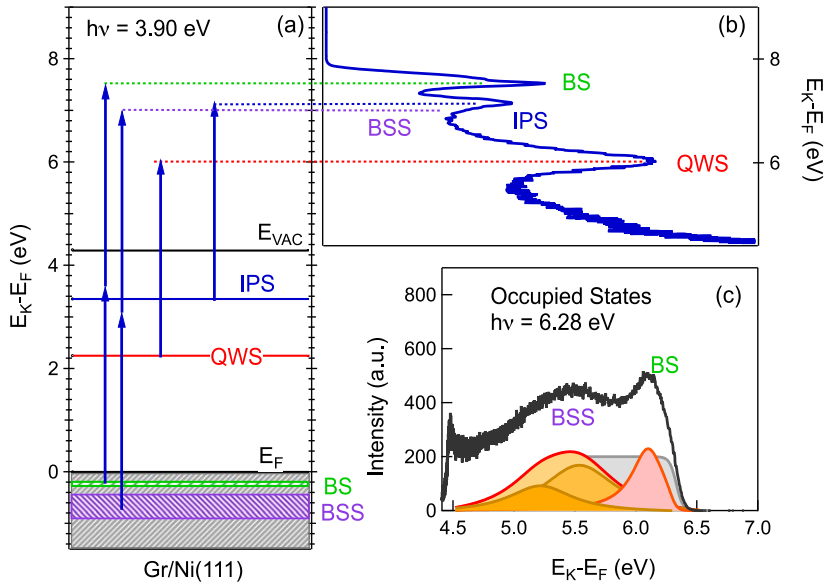

Figure 1. (a) Sketch of the graphene/Ni(111) electronic structures close to the Fermi level at the $\bar{\Gamma}$-point of the Brillouin zone. Vertical arrows indicate the expected excitation process responsible for the features in the 2-PPE photoemission spectrum. (b) Graphene/Ni (111) 2-PPE spectrum, as measured with *P*-polarized light at a photon energy of 3.90 eV and normal emission ($k_{\|} = 0$) geometry. (c) Linear photoemission spectrum collected with a photon energy of 6.28 eV. The shaded peaks are the Lorentzian curves used to fit each experimental feature, while the gray line shows the Fermi edge.

available photon energies allowed the investigation of the parallel crystal momentum in a range of ± 0.3 Å^{-1} around $k_{\|} = 0$ (normal emission). The angle of incidence of the laser beam with respect to the surface normal was $\theta = 30°$. Linear angle-resolved photoemission measurements on Ni(111) were collected using the fourth harmonics (6.28 eV) of a Ti-Sapphire oscillator, 80 MHz of repetition rate, and a VG-Scienta R3000 hemispherical electron analyser. All measurements were carried out at room temperature.

3. Theoretical model

The *ab initio* electronic structure calculations were carried out in density functional theory [28] within the generalized gradient approximation, employing the Perdew–Burke–Ernzerhof functional [29] to handle exchange and correlation effects. According to the self-consistent method implemented in the SIESTA code [30] the core electrons were described by a separable norm conserving pseudo-potential. The electronic wave function was expanded on a double-ζ polarized numerical orbital basis set. As suggested in [31], we have used enlarged cutoff radii for the basis function of Ni atoms. A symmetric slab with 52 Ni layers sandwiched by graphene was used for the calculation. For a better description of electronic surface states whose wave functions are spatially localized in vacuum, the basis set has been expanded in the vacuum region outside the graphene plane using Ni atomic orbitals and Bessel functions. The energy cutoff was fixed to 400 Ry and the Brillouin zone was sampled by a $12 \times 12 \times 1$ Monkhorst–Pack grid. The DOS was calculated on a six times denser mesh of *k*-points and a Gaussian smearing width of 0.02 eV.

The graphene layer was placed in both the top-fcc and top-bridge configuration with respect to the underneath Ni substrate. The Ni atoms of the outermost layer and the C atoms of the graphene plane were relaxed until the residual forces were smaller than 0.01 eV Å^{-1}, while the cells size was maintained constant during the calculation fixed by the Ni lattice constant ($a = 3.58$ Å). The optimized graphene-Ni distance resulted equal to 2.07 Å and 2.09 Å for the top-bridge and top-fcc configuration, respectively.

4. Results and discussion

Figure 1(a) shows the electronic transitions giving rise to the features of the 2-PPE spectrum reported in figure 1(b) and collected on graphene/Ni(111) with a photon energy of 3.90 eV, with *P*-polarized light and at normal emission ($k_{\|} = 0$). Being the kinetic energy (E_K) referred to the Fermi level, the edge at $E_K \sim 7.8$ eV in figure 1(b) represents the emission from E_F by two-photon absorption. Three main features, labeled as QWS ($E_K \sim 6$ eV), IPS ($E_K \sim 7.2$ eV), and BS ($E_K \sim 7.5$ eV), are observed. To identify the structures belonging to the occupied electronic states, a linear photoemission spectrum, using $h\nu = 6.28$ eV and mainly *P*-polarized

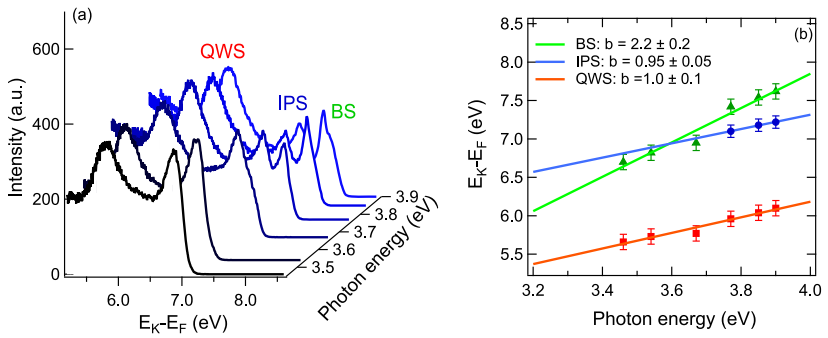

Figure 2. (a) Graphene/Ni(111) 2-PPE spectra collected by tuning the photon energy across the BS-IPS transition (from 3.4 to 3.9 eV), at normal emission ($k_{||} = 0$) and with *P*-polarized light. (b) Kinetic energy of the IPS, SS, and QWS features versus pump photon energy and linear fit to determine the number of photons (*b* values) involved in the photoemission process. The point where the two lines cross corresponds to the BS-IPS transition energy.

photons at $k_{||} = 0$ (figure 1(c)), was collected. The structure at $E_K \sim 6$ eV in figure 1(c) will be identified as the BS state of the 2-PPE spectrum, while a new wide feature labeled as BSS at $E_K \sim 5.4$ eV appears. The structures observed in the spectra have been fitted with a Lorentzian convoluted with a Gaussian function accounting for the experimental resolution (35 meV). For all the measured features, except BS, two Lorentzians are necessary to adequately fit the corresponding peak. This suggests that, conversely to the BS structure, two spin components contribute to the IPS, QWS, and BSS photoemission signals. In particular, the last one is very broad and the two spin components, shown in figure 1(c), are about 350 meV apart, while the exchange splitting for QWS and IPS (not shown in the figure) amount to 150 meV and 80 meV, respectively. It is worth noting that the narrowness of the BS feature could be due to the cut induced by the Fermi edge at 6.28 eV. Comparing the two spectra reported in figures 1(b) and (c) we assess that BS and BSS are occupied states with energy of -0.25 ± 0.05 eV and -0.85 ± 0.05 eV with respect to the Fermi level. The BSS state is not visible in figure 1(b) because it lies below the IPS signal.

Differently, QWS and IPS are unoccupied states and their energies, referred to the Fermi level, are 2.15 ± 0.05 eV and 3.3 ± 0.05 eV, respectively. We ascribe the IPS to the $n = 1$ IPS and its binding energy with respect to the vacuum level results 0.95 ± 0.1 eV.

The scenario proposed above for the surface states is confirmed by collecting the 2-PPE spectra tuning the laser photon energy from 3.4 to 3.9 eV (figure 2(a)) and tracking the energy position of IPS and BS versus the photon energy (figure 2(b)). In these spectra, the occupied BSS merges in the background due to its broadness and to the presence of the IPS and QWS competitive channels. As expected, the energy position of the unoccupied QWS and IPS shifts as the laser photon energy ($1\Delta h\nu$), while the occupied BS shifts with twice the photon energy ($2\Delta h\nu$). As can be observed in figure 2(a), the IPS feature can be detected only by using photon energies larger than 3.55 eV that corresponds to the transition from BS to IPS. At this photon energy, we do not observe a strong increase of the IPS photoemission intensity. The absence of a clear resonance suggests that the BS structure is not a surface state. Surface state electrons, in fact, compared to electrons in bulk states are more likely to be laser-excited into the image potential since both, surface and IPS have a high probability density at the surface and thus large spatial overlap. This causes a significantly higher 2-PPE intensity if the photon energy is resonant with the energy difference between an occupied surface and the IPS [32].

In order to demonstrate that the occupied BS structure is the Nickel *d*-band, we have collected linear photoemission measurements ($h\nu = 6.28$ eV) on polished Ni(111). In figure 3(a), the comparison between the linear photoemission spectra of Ni(111) and graphene/Ni(111) at the $\overline{\Gamma}$ point for both *S* and *P* polarization is reported. The spectra have been reported in kinetic energy referred to the Fermi level, evidencing the difference in the work function that we estimate equal to 5.5 eV for Ni(111) and 4.25 eV for graphene/Ni(111).

The measurements performed with *P*-polarized light on Ni(111) (black line) show two structures at 90 ± 5 meV and 260 ± 5 meV from the Fermi edge that can be attributed to the two surface features of Ni(111), namely S1 in the majority component and S2 in the minority one, already reported in literature [17]. This is consistent with the capability of *P*-polarized photons to evidence surface specific features. Differently, the *S*-polarized light produces a photoemission spectrum for Ni(111) (black line) characterized by only one feature at 200 meV below the Fermi energy, which is intermediate with respect to that of the features observed with *P*-polarized photons. Because *S*-polarization does not allow photoemission from pure surface states, we attribute the observed peak to the minority spin *d*-band of Ni. The spectra relative to graphene/Ni(111) display only one broad feature, corresponding to the BS state, that is unchanged by varying the polarization. As a consequence, we ascribe the latter to the *d*-band of Ni. The *d*-band collected by using a photon energy of 6.28 eV appears much

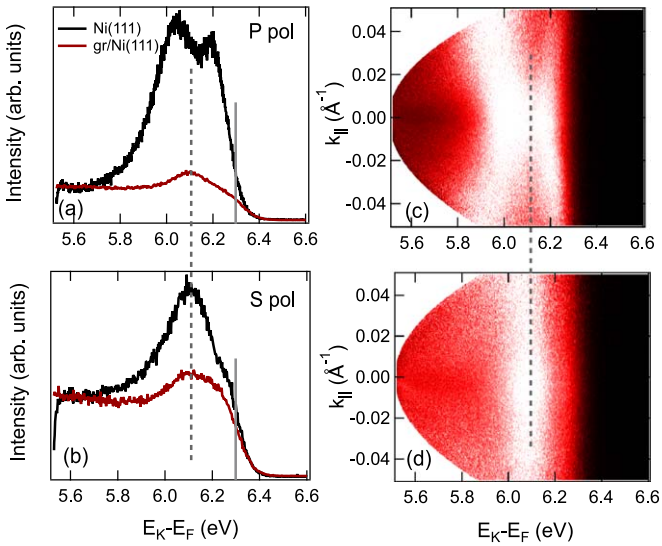

Figure 3. (a)–(b): Comparison between the linear photoemission spectra of Ni(111) (black line) and graphene/Ni(111) (red line) collected by a photon energy of 6.28 eV at the $\overline{\Gamma}$ point for both *P*- and *S*-polarization. (c)–(d): $k_{||}$ resolved linear photoemission spectra of Ni(111) for *P*- and *S*-polarization. The Fermi edge, at 6.28 eV, is marked by a solid gray line.

narrower than the valence *d*-band collected by using photon energies of tens of eV, for example using a He lamp (see the supplementary material available online at stacks.iop.org/NJP/20/103039/mmedia).

In this light, we can state that the presence of graphene on Ni(111) clears away from the surface states the electronic structure close to the Fermi level, leaving, at the $\overline{\Gamma}$ point, only spin selected states belonging to the minority *d*-band.

From angle-resolved photoemission data, it is possible to track the $k_{||}$-dispersion for the Ni(111) surface states and for both occupied and unoccupied states of graphene/Ni(111) (see the supplementary material). The Ni(111) S1 state disperses, as expected [17], toward the Fermi energy, forming an electron pocket, with an effective mass equals to $0.42 \pm 0.02\ m_e$, whereas the dispersion of the S2 state is hole-like with $m^* = -0.33 \pm 0.02\ m_e$. The QWS shows an effective mass of about $0.6 \pm 0.02\ m_e$. The IPS effective mass confirms the free electron like character of this state being $m^* = 1.1 \pm 0.02\ m_e$.

This value completes the characterization of the $n = 1$ IPS on graphene/Ni(111). The IPS binding energy (0.95 ± 0.1 eV) could be compared with the $n = 1$ IPS (0.80 ± 0.03 eV) measured on clean Ni(111) [33] and 0.74 ± 0.03 eV on a similar interface (graphene/Au/Ni(111)) [13, 34]. We note that the binding energy of the graphene/Ni(111) $n = 1$ IPS, here measured, results in disagreement with previous theoretical predictions (0.41 eV) [35].

It is worth noting that a theoretical description of IPS needs to reproduce the long range decay of the image potential tail in vacuum, a requirement not accomplished by density functional theory treatment. Different possible alternatives, less demanding than a many body approach, have been adopted, such as an empirical correction to the *ab initio* potential in vacuum [36] or more simplified one dimensional models [37]. IPSs of graphene on noble metal surfaces were calculated through a Thomas–Fermi theory applied to a 1D potential. These calculations show that there is a relationship between the screening length of the supported graphene, the charge transfer and the binding energy of the IPS [34, 38]. An alternative approach has been proposed by Armbrust *et al* [39] that exploit an analytical model potential for graphene on metals showing that the IPS binding energy is essentially determined by the graphene-metal distance. Following this model the IPS of graphene/Ni(111) is expected to behave approximatively as that of graphene/Ru(0001) in the regions of strong interaction, i.e. small equilibrium distance. Nevertheless these models work well for weakly interacting graphene/metal systems in which the charge density of graphene due to the doping level can be related, through a simple analytical equation [40], to the difference of the work functions between graphene and the substrate and to their mutual distance. For strongly interacting graphene/metal systems, in which the chemical interaction between the overlayer and the substrate significantly modifies the electronic properties of the whole system with respect to the pristine ones, this model is not well grounded.

To assess the scenario of the states at the graphene/Ni(111) interface, the DOS and the band structure have been calculated by a density functional theory approach and are reported in figure 4. The surface features in the band structure are highlighted in red, while different colors in the DOS correspond to the projection on different atoms in the system. We consider both the top-fcc (top panel) and the top-bridge (bottom panel) graphene

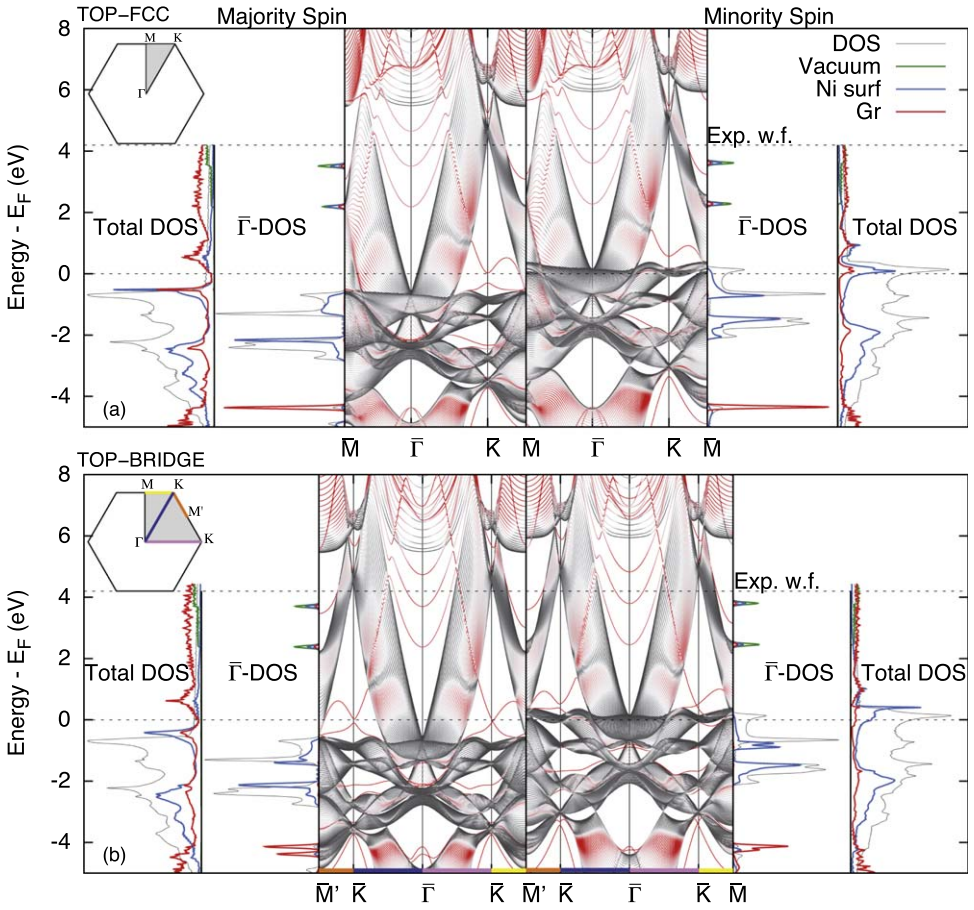

Figure 4. Density of state and band structure of graphene/Ni(111) in the top-fcc (top panel) and top-bridge (bottom panel) stacking. The total DOS and the DOS at the $\overline{\Gamma}$ point of the two spin components are reported in the lateral panels with different colors, corresponding to projection on different atoms/volumes. In the majority (left) and minority (right) spin band structures and DOS the graphene states have been highlighted in red.

Table 1. Experimental and theoretical energies of the surface states of graphene/Ni(111) with respect to the Fermi level. Energies in parenthesis are referred to the vacuum level.

	Energy (eV)					Effective Mass (m_e)		
	Exp	top-bridge		top-fcc		Exp	top-bridge	top-fcc
		up	dw	up	dw			
BSS	−0.85	−1.42	−0.89/−0.77 [a]	−1.3[a]	−0.72	—	—	—
BS	−0.25	—	*d*-band	—	*d*-band	—	—	—
QWS	2.15	2.35	2.45	2.17	2.26	0.6	0.6	0.72
IPS	3.30 (−0.95)	3.68	3.80	3.50	3.60	1.1	—	—

[a] Resonance state.

stacking. Note that, in the latter the irreducible Brillouin zone is larger compared to that of Ni(111), due to the lacking of C_3 symmetry in the system (while the C_2 symmetry is preserved). As highlighted in the inset, the $\overline{\mathrm{K}}\,\overline{\mathrm{M}}$ and $\overline{\mathrm{K}}\,\overline{\mathrm{M}}'$ high symmetry paths are no more equivalent.

Differently, in the top-fcc stacking the C_3 symmetry is preserved but the two carbon atoms are not equivalent being one on top of the Ni atom and the other in the fcc position. The broken symmetry between *A* and *B* graphene sublattices gives rise to the opening of energy gaps in correspondence of the Dirac cones at the Fermi level and below [41], that are absent in the top-bridge stacking where the Dirac cone is preserved. The theoretical binding energies of the surface features at the $\overline{\Gamma}$ point are reported in table 1.

Concerning the occupied states, our theoretical calculations confirm the experimental finding. At the $\overline{\Gamma}$ point we do not find any evidence of surface state at −0.25 eV. In this energy range there is instead the minority spin band of Ni related to BS feature. The BSS is originated by a downward dispersing surface state which is

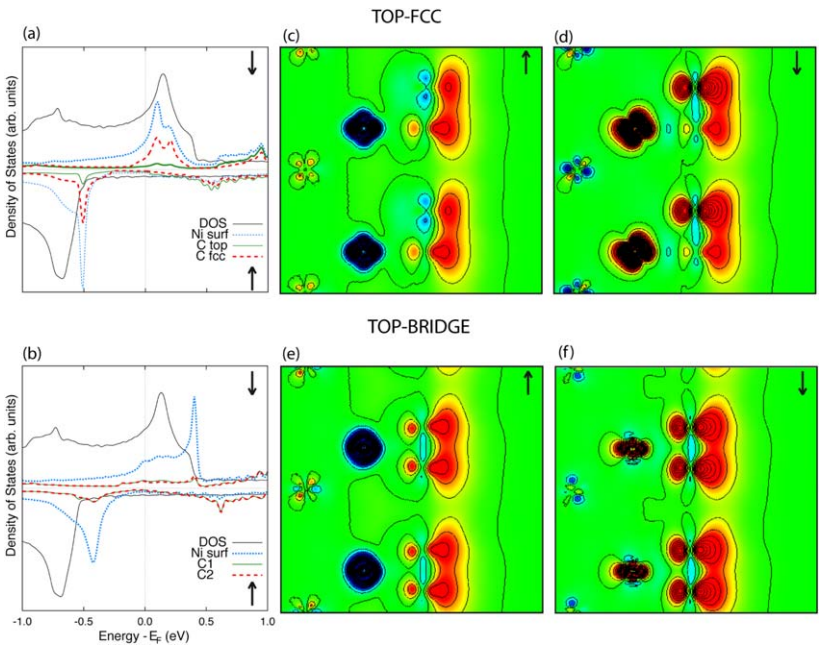

Figure 5. (a)–(b) Density of states of the top-fcc and top-bridge configuration, projected onto different atomic volumes. (c)–(f) Induced screening charge density on a plane passing through the two carbon atoms in the unit cell and the outermost Ni atom. Top panel: top-fcc stacking for the majority (right) and minority (left) spin component. Bottom panel: the same for the top-bridge stacking. Red (blue) color corresponds to a reduction (increase) of charge upon application of the electric field, the green color is the reference zero density.

shifted at higher binding energy with respect to S2 state of clean Ni(111). In the top-fcc configuration its majority component results hybridized with the *d*-band while the minority one retains its surface state character lying in the energy gap. In the top-bridge stacking both the spin components can be identified at the $\overline{\Gamma}$ point. Notably in the top-bridge stacking the BSS is split in two peaks for each spin component. One of the two spin contributions is below the *d*-band, lying in the gap, and it results more visible in the photoemission spectrum. The lifted degeneracy characterizes also the surface states at lower energy, as for example the feature at -4.2 eV. The exchange splitting between majority and minority spin BSS is comparable to the experimental one (see table 1).

The calculated QWS displays at the $\overline{\Gamma}$ point an energy (with respect to E_F) of 2.17 eV and 2.35 eV for the majority spin component in the top-fcc and top-bridge geometry, respectively. The exchange splitting of QWS at $\overline{\Gamma}$ is 0.1 and 0.09 eV for the two configurations. The effective masses of the QWS, estimated by a parabolic fit in the $(-0.15, 0.15)$ Å^{-1} $k_{||}$ range, are slightly different, being equal to 0.6 m_e in the top-bridge and 0.72 m_e in the top-fcc, as expected due to the slightly different energy position of QWS in the gap.

The comparison between the band structures of the graphene-covered Ni(111) and that of the clean surface (see the supplementary material) sets that the unoccupied QWS is originated from the occupied S1 majority spin surface state of Ni(111) that results upward shifted in energy due to the interaction with the graphene layer. This assignment is supported also by the projected DOS in different volumes showing that this state is spatially localized on the Ni surface layer (purple line), as usually happens for the Shockley surface state.

The DOS and band structure display also a surface feature at about 3.9 eV above the Fermi level that cannot be directly compared with the IPS because it is generated by a potential which does not appropriately include the image potential tail. Although a precise description of IPS is precluded by the adopted formalism, *ab initio* calculations can give information about the screening properties of the system, that are directly related to the formation of the IPS.

In order to address the differences between the two possible local arrangements of graphene on Ni(111), we have calculated the response of both the top-fcc and the top-bridge stacking to a small external electric field. We consider the induced screening charge density which is reported in figures 5(c)–(f) for the two spin components. The 2D plot has been obtained selecting a plane passing through the two carbon atoms and the outermost Ni surface atom. Although the Ni contribution remains higher, graphene contributes significantly to the screening. The induced screening charge density is mainly due to the minority spin states that outnumber the majority ones at the Fermi level, as shown in figures 5(a) and (b) in which an enlargement of the DOS is reported, also projected on the three atoms that identify the plane for the 2D plot. Moreover, the top-fcc stacking is characterized by a major contribution of the carbon atom in the fcc position with respect to that adsorbed on top. Differently, in the top-bridge configuration the two carbon atoms contribute equivalently. Although both the spin and spatial

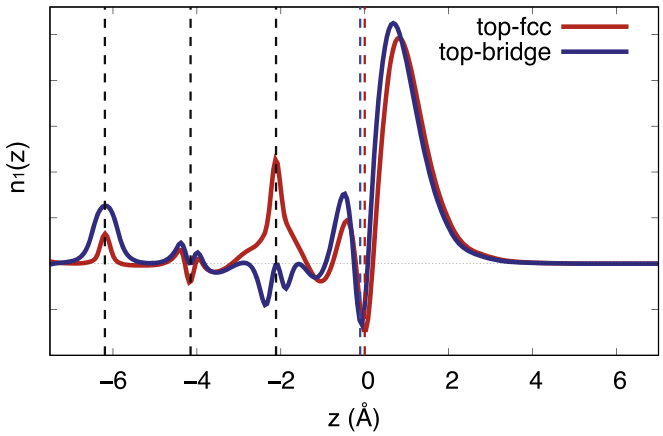

Figure 6. First-order induced density $n_1(z)$ for the top-fcc (red) and top-bridge (blue) stacking. Vertical dashed lines give the position of the atomic planes.

descriptions of the induced screening charge density evidence some differences in the two stackings, these ones are almost completely lost in the overall response to the electric field which is reported in figure 6 as the normalized planar average of the total induced screening charge density $n_1(z)$ [36], as a function of z, normal to the surface.

In particular, figure 6 shows that the graphene contribution to the response function is only slightly larger in the top-bridge configuration. The image plane can be obtained as centroid of $n_1(z)$ [36]:

$$z_{\rm im} = \int_{-\infty}^{\infty} z\, n_1(z)\,{\rm d}z, \qquad \text{where} \qquad \int_{-\infty}^{\infty} n_1(z)\,{\rm d}z = 1. \tag{1}$$

Due to the similarity of the two curves it results almost equal to 1 Å for both the stackings. This implies that the binding energy of the IPS does not depend on the arrangement of graphene with respect to the substrate.

5. Conclusions

By a joint effort of linear and nonlinear photoemission measurements and *ab initio* calculations, we characterize the electronic states at the graphene/Ni(111) interface. The presence of graphene frees the occupied *d*-band from the two Ni surface states. One shifts in the gap becoming an unoccupied state (QWS) and the other at higher binding energy (BSS) with respect to the Fermi level. The image state, despite the small distance between the graphene layer and the Ni surface, seems to preserve its properties. The binding energy results, in fact, more similar to that of Ni(111) rather than to the predicted theoretical value [35]. The one-potential models, reported in literature to calculate energies and wave functions of the unoccupied interface states, are able to reproduce the experimental data of weakly interacting graphene/metal interfaces. Graphene/Ni(111), as underlined in the introduction, is a model system for strongly interacting systems and the experimental results here reported require that the models, so far proposed, have to be revised when graphene strongly interacts with the substrate.

ORCID iDs

C Cepek https://orcid.org/0000-0002-9195-7611
C Africh https://orcid.org/0000-0002-1922-2557

References

[1] Voloshina E N and Dedkov Y S 2014 *Mater. Res. Express* **1** 4465
[2] Batzill M 2012 *Surf. Sci. Rep.* **67** 83–115
[3] Pletikosić I, Kralj M, Pervan P, Brako R, Coraux J, N'Diaye A T, Busse C and Michely T 2009 *Phys. Rev. Lett.* **102** 056808
[4] Varykhalov A, Marchenko D, Sánchez-Barriga J, Scholz M R, Verberck B, Trauzettel B, Wehling T O, Carbone C and Rader O 2012 *Phys. Rev.* X **2** 041017
[5] Karpan V M, Giovannetti G, Khomyakov P A, Talanana M, Starikov A A, Zwierzycki M, van den Brink J, Brocks G and Kelly P J 2007 *Phys. Rev. Lett.* **99** 176602
[6] Karpan V M, Khomyakov P A, Starikov A A, Giovannetti G, Zwierzycki M, Talanana M, Brocks G, van den Brink J and Kelly P J 2008 *Phys. Rev.* B **78** 195419
[7] Zhang W B, Chen C and Tang P Y 2014 *J. Chem. Phys.* **141** 044708

[8] Dedkov Y S and Fonin M 2010 *New J. Phys.* **12** 125004
[9] Maassen J, Ji W and Guo H 2011 *Nano Lett.* **11** 151–5
[10] Bertoni G, Calmels L, Altibelli A and Serin V 2005 *Phys. Rev.* B **71** 075402
[11] Pagliara S, Tognolini S, Bignardi L, Galimberti G, Achilli S, Trioni M I, van Dorp W F, Ocelík V, Rudolf P and Parmigiani F 2015 *Phys. Rev.* B **91** 195440
[12] Tognolini S, Achilli S, Longetti L, Fava E, Mariani C, Trioni M I and Pagliara S 2015 *Phys. Rev. Lett.* **115** 046801
[13] Niesner D 2013 Two-photon photoemission studies of graphene and topological insulators *PhD Thesis* Naturwissenschaftlichen Fakultät der Friedrich-Alexander-Universität Erlangen-Nürnberg
[14] Armbrust N, Güdde J, Jakob P and Höfer U 2012 *Phys. Rev. Lett.* **108** 056801
[15] Voloshina E and Dedkov Y 2012 *Phys. Chem. Chem. Phys.* **14** 13502–14
[16] Andres B, Weiss P, Wietstruk M and Weinelt M 2015 *J. Phys.: Condens. Matter* **27** 015503
[17] Lobo-Checa J, Okuda T, Hengsberger M, Patthey L, Greber T, Blaha P and Osterwalder J 2008 *Phys. Rev.* B **77** 075415
[18] Ohwaki T, Wortmann D, Ishida H, Blügel S and Terakura K 2006 *Phys. Rev.* B **73** 235424
[19] Okuda T *et al* 2009 *Phys. Rev.* B **80** 180404(R)
[20] Fuentes-Cabrera M, Baskes M I, Melechko A V and Simpson M L 2008 *Phys. Rev.* B **77** 035405
[21] Hermanns C F, Tarafder K, Bernien M, Krüger A, Chang Y, Oppeneer P M and Kuch W 2013 *Adv. Mater.* **25** 3473–7
[22] Sun X, Entani S, Yamauchi Y, Pratt A and Kurahashi M 2013 *J. Appl. Phys.* **114** 143713
[23] Zhao W, Kozlov S M, Höfert O, Gotterbarm K, Lorenz M P A, Viñes F, Papp C, Görling A and Steinrück H 2001 *J. Phys. Chem. Lett.* **2** 759–64
[24] Kozlov S, Viñes F and Görling A 2012 *J. Phys. Chem.* C **116** 7360–6
[25] Bianchini F, Patera L, Peressi M, Africh C and Comelli G 2014 *J. Phys. Chem. Lett.* **5** 467–73
[26] Lahiri J, Lin Y, Bozkurt P, Oleynik I I and Batzill M 2010 *Nat. Nanotechnol.* **5** 326–9
[27] Patera L L *et al* 2013 *ACS Nano* **7** 7901
[28] Hohenberg P and Kohn W 1964 *Phys. Rev.* **136** B864
[29] Perdew J P, Burke K and Ernzerhof M 1996 *Phys. Rev. Lett.* **77** 3865
[30] Soler J M, Artacho E, Gale J D, Garcia A, Junquera J, Ordejon P and Sánchez-Portal D 2002 *J. Phys.: Condens. Matter* **14** 2745
[31] Santos E J G, Ayuela A and Sánchez-Portal D 2012 *New J. Phys.* **12** 053012
[32] Tognolini S, Achilli S, Ponzoni S, Longetti L, Mariani C, Trioni M and Pagliara S 2018 *Surf. Sci.* **679** 11–6
[33] Schuppler S, Fischer N, Steinmann W, Schneider R and Bertel E 1990 *Phys. Rev.* B **42** 9403
[34] Nobis D, Potenz M, Niesner D and Fauster T 2013 *Phys. Rev.* B **88** 195435
[35] Güdde J, Berthold W and Höfer U 2006 *Chem. Rev.* **106** 4261–80
[36] Achilli S, Caravati S and Trioni M I 2007 *Surf. Sci.* **601** 4048–52
[37] Chulkov E V, Silkin V M and Echenique P M 1999 *Surf. Sci.* **437** 330–52
[38] de Andres P L, Echenique P M, Niesner D, Fauster T and Rivacoba A 2012 *New. J. Phys.* **16** 023012
[39] Armbrust N, Güdde J and Höfer U 2015 *New J. Phys.* **17** 103043
[40] Giovannetti G, Khomyakov P A, Brocks G, Karpan V M, van den Brink J and Kelly P J 2008 *Phys. Rev. Lett.* **101** 026803
[41] Martinazzo R, Casolo S and Tantardini G F 2010 *Phys. Rev.* B **81** 245420